Supersaturated bridge-sulfur and vanadium co-doped MoS_2 nanosheet arrays with enhanced sodium storage capability

Yuru Dong[1, #], Zhengju Zhu[1, #], Yanjie Hu[1, *], Guanjie He[2], Yue Sun[1], Qilin Cheng[1], Ivan P. Parkin[2], Hao Jiang[1, *]

[1] *Key Laboratory for Ultrafine Materials of Ministry of Education, Shanghai Engineering Research Center of Hierarchical Nanomaterials, School of Materials Science and Engineering, East China University of Science & Technology, Shanghai 200237, China*

[2] *Christopher Ingold Laboratory, Department of Chemistry, University College London, 20 Gordon Street, London WC1H 0AJ, U.K.*

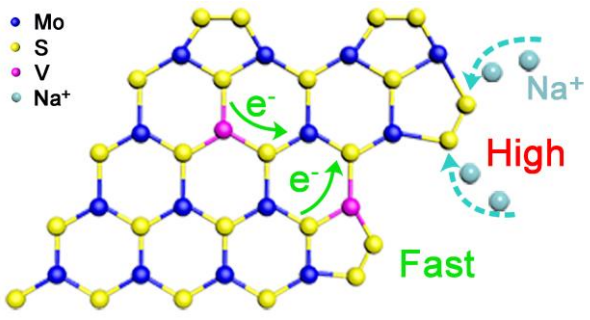

The supersaturated bridge-sulfur and vanadium co-doped MoS_2 nanosheet delivers ultrahigh sodium storage capacity and fast reaction kinetics.

Nano Research

ISSN 1998-0124 CN 11-5974/O4
https://doi.org/(automatically inserted by the publisher)

Research Article

Supersaturated bridge-sulfur and vanadium co-doped MoS_2 nanosheet arrays with enhanced sodium storage capability

Yuru Dong[1, #], Zhengju Zhu[1, #], Yanjie Hu[1] (✉), Guanjie He[2], Yue Sun[1], Qilin Cheng[1], Ivan P. Parkin[2], and Hao Jiang[1] (✉)

[1] *Key Laboratory for Ultrafine Materials of Ministry of Education, Shanghai Engineering Research Center of Hierarchical Nanomaterials, School of Materials Science and Engineering, East China University of Science & Technology, Shanghai 200237, China*
[2] *Christopher Ingold Laboratory, Department of Chemistry, University College London, 20 Gordon Street, London WC1H 0AJ, U.K.*
[#] *Yuru Dong and Zhengju Zhu contributed equally to this work.*

Received: day month year / **Revised:** day month year / **Accepted:** day month year (automatically inserted by the publisher)

ABSTRACT

The low specific capacity and sluggish electrochemical reaction kinetics greatly block the development of sodium-ion batteries (SIBs). New high-performance electrode materials will enhance development and are urgently required for SIBs. Herein, we report the preparation of supersaturated bridge-sulfur and vanadium co-doped MoS_2 nanosheet arrays on carbon cloth (denoted as V-MoS_{2+x}/CC). The bridge-sulfur in MoS_2 has been created as a new active site for greater Na^+ storage. The vanadium doping increases the density of carriers and facilitates accelerated electron transfer. The synergistic dual-doping effects endow the V-MoS_{2+x}/CC anodes with high sodium storage performance. The optimized V-$MoS_{2.49}$/CC gives superhigh capacities of 370 and 214 mAh g^{-1} at 0.1 and 10 A g^{-1} within 0.4-3.0 V, respectively. After cycling 3000 times at 2 A g^{-1}, almost 83% of the reversible capacity is maintained. The findings indicate that the electrochemical performances of metal sulfides can be further improved by edge-engineering and lattice-doping co-modification concept.

KEYWORDS

MoS_2, bridge sulfur, high specific capacity, sodium-ion battery, cycle life

1 Introduction

Rechargeable sodium ion batteries (SIBs) as replacement candidates for lithium ion batteries (LIBs) have been intensively investigated in view of abundant sodium resource, high economic benefits, and sodium-free dendrites [1-4]. However, owing to the weaker binding to the substrate and larger radius of Na^+ compared to Li^+, commercial graphite for lithium-ion batteries exhibits obvious thermodynamic and kinetic deficiencies for sodium storage [5-7]. Therefore, exploiting new high-performance electrode materials is pivotal in promoting practical application of SIBs. In recent years, two-dimensional (2D) molybdenum disulfide (MoS_2) has been considered as a promising anode material for SIBs due to its large interlayer distance (0.62 nm), weak van der Waals forces and four electrons conversion reactions enabling facile Na^+ insertion/extraction and contributing to a high theoretical specific capacity (e.g. 670 mAh g^{-1}) [8-12]. Nevertheless, the conversion reaction below 0.4 V is usually accompanied by non-negligible volume changes and the dissolution of intermediate polysulfides, consequentially leading to structure pulverization and rapid capacity decay [13,14]. Although manipulating the cut-off voltage to guarantee the intercalation reaction above 0.4 V is able to improve the cycling stability [15-17], the loss of conversion reaction engenders a sacrifice of theoretical capacity [18]. Thus, it is of great importance to promote the specific capacity of intercalation-type MoS_2 electrodes. Furthermore, the poor intrinsic conductivity of thermodynamically stable 2H-MoS_2 also impedes its fast-charging performance [8, 19].

To increase the specific capacity of intercalation-type MoS_2, great endeavors have been taken to engineer the MoS_2 into fewer layers, decrease the size of nano-scale MoS_2 and expand its interlayer distance [8, 9, 13, 15]. Despite the considerable progress that has been achieved via the above methods, only a small amount of attention has been paid to design and tune the atomic structure of MoS_2 to enhance the practical specific capacity. Recently, some groups demonstrated that the bridge sulfur in MoS_2 is the major active site for the hydrogen evolution reaction (HER), outperforming the terminal sulfur [20-22]. However, to our knowledge, there have been no studies that utilize bridge sulfur to modify MoS_2 for SIBs. Based on the understanding of the mechanism of Na-S battery, we believe that the bridge sulfur could possibly act in a similar way to S_8 or polysulfides, which means that the bridge sulfur can react with Na^+ to realize a reversible conversion between bridge sulfur and sodium sulfide (Na_2S) [23-25]. Interestingly, the reduction reaction of S needs a higher voltage than that to break the Mo-S bond during the initial discharging process [13, 25]. Therefore, introducing bridge sulfur is promising as a modifier to improve the capacity of MoS_2 electrodes when cycling at above 0.4 V. On the other hand, to optimize the electron transportation ability, the most common protocol focuses on coupling the high-conductive carbon matrixes

Address correspondence to Yanjie Hu, huyanjie@ecust.edu.cn; Hao Jiang, jianghao@ecust.edu.cn

with MoS_2 [8,15]. Due to the existence of these carbon matrixes, the conductivity of the as-prepared nanocomposites is improved, but the intrinsic conductivity of MoS_2 is still untouched and unsatisfactory, which hampers the electron transfer capability in the plane and interlayer of MoS_2. Recent studies have revealed that element doping (e.g. Co, V) can effectively modulate the electronic structure of metal sulfides, thereby controlling their conductive behavior [26-28]. For example, Zhao et al. [27] found that pristine MoS_2 semiconductor showed through theoretical calculations that metallic characteristics with a bandgap of ~0 eV could be achieved by doping with Co. Thus, adopting a doping approach to realize the electronic structure engineering might be a promising strategy to optimize the intrinsic conductivity of MoS_2.

In this work, we have designed and prepared the supersaturated bridge-sulfur and vanadium co-doped MoS_2 nanosheet arrays on carbon cloth (labeled as V-MoS_{2+x}/CC) via a one-step hydrothermal method. The abundant bridge sulfur was successfully introduced into MoS_2 due to the addition of excess sulfur source, serving as active sites to receive Na^+ for providing extra specific capacity. Moreover, the vanadium doping can effectively tune the electronic structure and significantly improve the intrinsic conductivity of MoS_2 without destroying its lamellar structure. Benefiting from the synergistic effect between bridge-sulfur and vanadium doping, the optimized V-$MoS_{2.49}$/CC exhibits ultrahigh discharge capacities of 370 mAh g^{-1} at 0.1 A g^{-1}, and 214 mAh g^{-1} at 10 A g^{-1} in the 0.4-3.0 V range. More impressively, a capacity of 207 mAh g^{-1} (83% retention) is sustained after 3000 cycles with a low capacity decay of 0.005% per cycle at 2.0 A g^{-1}.

2 Experimental

2.1 Synthesis of the V-doped MoS_{2+x} on carbon cloth

Firstly, 0.5 g of $(NH_4)_6Mo_7O_{24}\cdot 4H_2O$ and 0.058 g of NH_4VO_3 were dissolved into 30 mL of deionized (DI) water. Then 1 mL of $NH_3\cdot H_2O$ was dropped into the solution under stirring. Different amounts of thioacetamide (TAA) from 0.2 to 1.5 g were added to synthesize a series of V-MoS_{2+x}/CC compositions. After vigorously stirring for another 1.5 h, the uniform mixture was transferred to a 50 mL autoclave with a piece of carbon cloth (9 cm^2, CeTech CO., LTD) and kept in an oven at 200 °C for 12 h. The final product was obtained by rinsing, drying and subsequent annealing at 300 °C for 2 h under Ar flow to remove small organic molecules. As controls, the pristine MoS_2 and MoS_{2+x} samples were prepared under the similar conditions by adding proper TAA in the absence of NH_4VO_3. The mass loading of active materials on the carbon cloth is 1.8 ~ 2 mg cm^{-2}.

2.2 Characterization

X-ray powder diffractometer (XRD, Bruker D8 Advance with Cu Kα radiation) was applied to characterize the crystal structure of the products. Raman spectra were record on Laser Micro-Raman Spectrometer. X-ray photoelectron spectroscopy (XPS) spectra were investigated on PHI 5000 Versa Probe. The molar proportions of the S in the samples were obtained using inductively coupled plasma mass spectrometry (ICP-MS; Agilent, ICP-7500). The electrical conductivities of the electrodes were measured using a four-point probe (model RTS-8, Guangzhou 4 Probes Tech Industrial Co., Ltd., Guangzhou, China). The morphology and microstructure were characterized by field emission scanning electron microscope (FESEM, S-4800) and transmission electron microscope (TEM, JEM-2100) with an X-ray energy dispersive spectrometer (EDS).

2.3 Electrochemical Measurements

Electrochemical measurements were performed using coin-type 2032 cells. The samples were cut into disks and then directly used as the working electrode. Pure sodium foil was employed as the counter electrode, and glass fiber membrane (Whatman) was used as the separator. 1 M $NaClO_4$ in ethylene carbonate (EC) and diethyl carbonate (DEC) (1:1 in volume) with 5 wt% fluoroethylene carbonate (FEC) was used as the electrolyte, which was purchased from MJS energy technology. Cyclic voltammetry (CV) tests from 0.4-3.0 V at various sweep rates and electrochemical impedance spectra (EIS) over a frequency range from 100 kHz to 0.01 Hz in a constant voltage mode were carried out on an Autolab PGSTAT302N. Galvanostatic charge/discharge behavior was measured by LAND CT2001A battery tester.

3 Results and discussion

Fig. 1 illustrates the designed concept of bridge-sulfur and doped V dual-modified MoS_2 (V-MoS_{2+x}/CC) nanosheet arrays on carbon cloth. Typically, during the hydrothermal process, thioacetamide (TAA, CH_3CSNH_2) acts as reducing agent and sulfur source based on the reaction of $CH_3CSNH_2 + 3OH^- \rightarrow CH_3COO^- + NH_3 + S^{2-} + H_2O$. The generated S^{2-} can further react with ammonium molybdate tetrahydrate (AMT) in stoichiometric proportions to form MoS_2 on the carbon cloth. When excessive TAA is added in the reaction system, the supersaturated S-S bonds (bridge sulfur) will be formed and further anchored on the surface of MoS_2 (denoted as MoS_{2+x}/CC), which can be as a new active site to storage more Na^+. In addition, the V-doped MoS_2 can be obtained via adding stoichiometric TAA and additional ammonium vanadate (NH_4VO_3), with the aim to compensate for the sluggish charge transfer kinetics of 2H-MoS_2. Unfortunately, there is only a single modification effect of MoS_2 in the aforementioned two composites, so it is hard to realize comprehensive improvement of electrochemical performances. Notably, the bridge-sulfur and vanadium doping co-modified MoS_2 (V-MoS_{2+x}/CC) can be synthesized by synchronously adding excess TAA and appropriate NH_4VO_3, integrating the advantages of the above two architectures, which will achieve high specific capacity and fast electrochemical reaction kinetics. The detailed evidence and corresponding discuss-

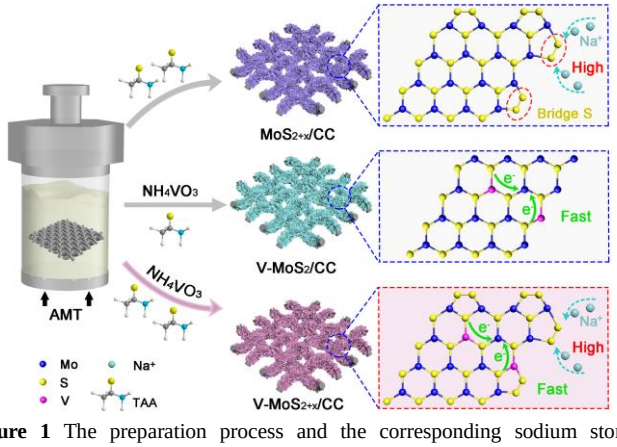

Figure 1 The preparation process and the corresponding sodium storage mechanism of the MoS_{2+x}/CC, the V-MoS_2/CC and the V-MoS_{2+x}/CC, respectively.

ion will be provided later. For comparison, pristine MoS_2 on the carbon cloth (MoS_2/CC) have been prepared under the similar condition without adding NH_4VO_3.

Firstly, a series of samples with different bridge-sulfur concentrations were prepared by changing the amount of TAA to make optimal V-MoS_{2+x}, which as shown by inductively coupled mass spectrometry (ICP-MS) where shown to be samples of composition V-MoS_2/CC, V-$MoS_{2.32}$/CC, V-$MoS_{2.49}$/CC, V-$MoS_{2.45}$/CC, and V-$MoS_{2.41}$/CC. Simultaneously, the mass ratio of V in the V-$MoS_{2.49}$/CC is about 2.1%. Afterwards, the elemental compositions and electronic states of the V-MoS_{2+x}/CC products were investigated by X-ray photoelectron spectroscopy (XPS). As seen in Fig. 2(a), the S 2p peaks from MoS_2/CC to V-$MoS_{2.41}$/CC first shift toward lower position then move to higher position with increasing x, suggesting that the conductivity firstly increases and then decreases [29-31]. The phenomenon of low-energy shifts can be ascribed to the anchoring of more electron-donating S atoms in the structure of V-MoS_{2+x}/CC. Impressively, the V-$MoS_{2.49}$ with the highest S content delivers the lowest peak position, demonstrating enhanced conductivity compared with other V-MoS_{2+x} hybrids. In addition, the results of deconvolved peaks indicate that the excess sulfur exists in the form of bridge sulfur (S-S) instead of the S^{2-} in MoS_2/CC [20, 21, 32]. The additional S-S bonds are expected to be new electrochemical active sites for providing high sodium storage. It is noteworthy that the bridge sulfur can be sustained even after annealing at 300 °C, implying strong combination between S-S bonds and MoS_2. Furthermore, the peak shifts in the Mo 3d spectra (Fig. 2(b)) also deliver an identical trend as the S 2p spectra, implying V-$MoS_{2.49}$ has the highest carrier concentration. The electrical conductivity is further quantified by four-point probe. As shown in Fig. 2(c), the conductivities of MoS_2/CC, V-MoS_2/CC, V-$MoS_{2.32}$/CC, V-$MoS_{2.49}$/CC, V-$MoS_{2.45}$/CC and V-$MoS_{2.41}$/CC are 13, 16, 21, 28, 12.6, and 11.3 S cm^{-1}, respectively, in accordance with above XPS analyses. X-ray diffraction (XRD) was also performed to uncover the impacts of S content and vanadium doping on the crystal structures of the V-MoS_{2+x}. As shown in Fig. 2(d), all of the peaks are matched to the pure MoS_2 phase, suggesting that vanadium element is doped in the crystal latticce rather than forming a secondary phase. This fact is also confirmed by the Raman spectrum of V-$MoS_{2.49}$/CC (see Fig. S1 in the ESM), where no characteristic peaks are related to the vibration modes of V-S bonds (140, 190, 280 cm^{-1}) [33]. Noteworthily, the intensities of (002) peaks in the V-MoS_{2+x}/CC strengthen gradually with the increasing of TAA, indicating enhanced crystallinity [34,35], which is detrimental to the formation of bridge sulfur and the doping of vanadium. As a result, the sulfur content and conductivity decrease after unduly increasing the amount of TAA. It can also be demonstrated by the V 2p spectrum that generation of pentavalent vanadium (Fig. 2(e)), which results from the oxidation of unstable V^{4+} on the surface during the hydrothermal process because the doping of V element in the lattice of MoS_2 becomes more difficult. As a consequence, it has been verified that the adding of the correct amounts of TAA and NH_4VO_3 can effectively tune the atomic structures of MoS_2 to create additional bridge sulfurs and regulate the conductivity, which are favorable for improving sodium storage performance.

The detailed morphology and microstructure information of the optimized V-$MoS_{2.49}$/CC were further characterized. The SEM analysis shown in Figs. 3(a)-3(b)) indicate that the carbon cloth is covered by uniformly grown nanosheets with vertical orientation. This can facilitate the penetration of electrolyte and the exposure of active surface. Specially, the morphology of V-$MoS_{2.49}$ is similar to that of the pristine MoS_2 (see Fig. S2 in the ESM), demonstrating that vanadium doping does not destroy the typical 2D structure of MoS_2. Furthermore, the high-magnification transmission electron microscopy (TEM) image (Fig. 3(c)) demonstrates that the nanosheet possesses an interlayer spacing of 0.64 nm, which is indexed to the typical 2H-MoS_2. The corresponding selected area electron diffraction (SAED) analysis (the inset of Fig. 3(c)) also certifies that the crystal phase of MoS_2 is present without other detectable impurities, in agreement with the XRD result. As shown in Figs. 3(d)-3(g), the TEM-EDS mapping of the V-$MoS_{2.49}$ demonstrates uniform distribution of Mo, V and S elements, supporting the homogeneous doping of V.

Motivated by the above structural and compositional design, the sodium storage performances of all the samples were evaluated by

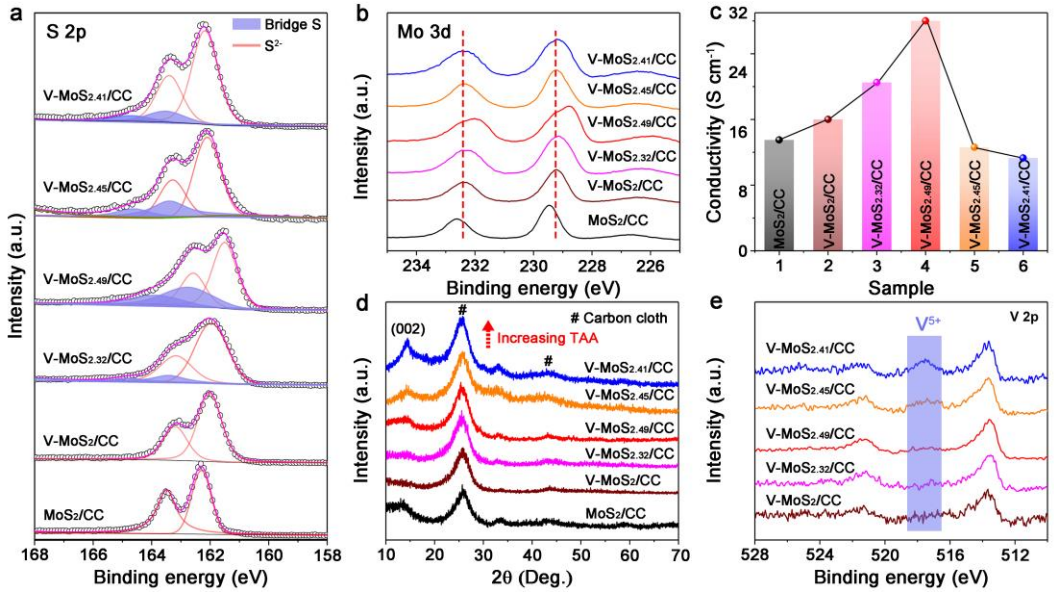

Figure 2 (a) S 2p and (b) Mo 3d XPS spectra, (c) the electronic conductivity, (d) XRD patterns, and (e) V 2p XPS spectra of the MoS_2/CC, the V-MoS_2/CC, the V-$MoS_{2.32}$/CC, the V-$MoS_{2.49}$/CC, the V-$MoS_{2.45}$/CC and the V-$MoS_{2.41}$/CC, respectively.

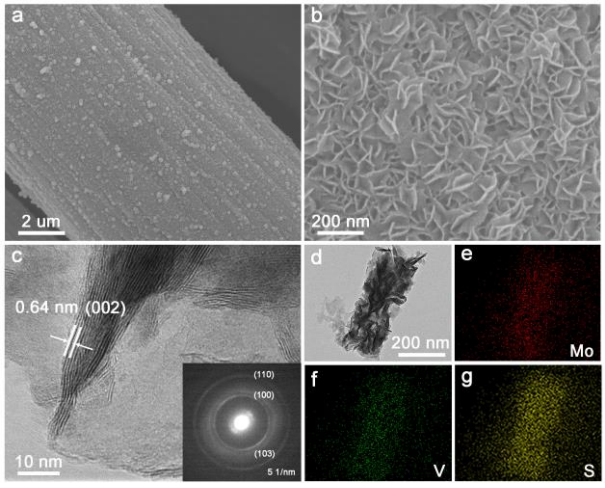

Figure 3 (a-b) SEM images, (c) TEM image (inset showing the corresponding SAED pattern), and (d-g) TEM-EDS mapping of Mo, V, and S elements of the V-$MoS_{2.49}$/CC.

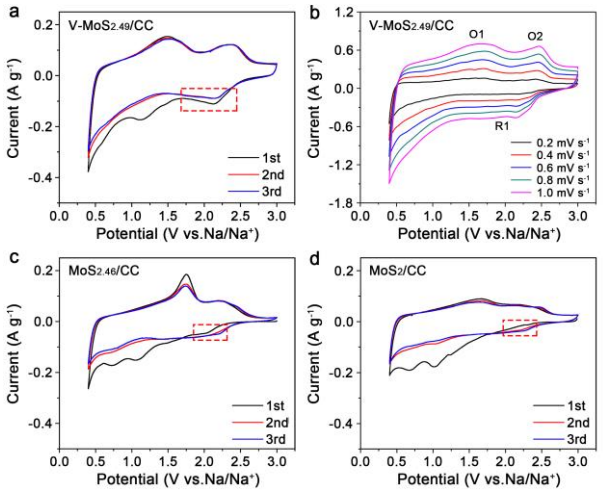

Figure 4 (a) The initial three CV curves and (b) the CV curves at 0.2-1.0 mV s^{-1} of the V-$MoS_{2.49}$/CC; (c-d) the initial three CV curves of the $MoS_{2.46}$/CC and the MoS_2/CC, respectively.

directly using them as anodes to assemble the 2032 coin-type half cells. As predicted, the V-$MoS_{2.49}$/CC indeed delivers an optimal electrochemical performance among all the V-MoS_{2+x}/CC samples (see Fig. S3 in the ESM) over the potential range of 0.4-3.0 V. Interestingly, the sodium storage capacities were enhanced in order of increasing S content, suggesting that bridge sulfur plays a significant role in the regulation of the electrochemical properties. To qualitatively reveal the effects of the bridge sulfur and vanadium doping, cyclic voltammetry (CV) was carried out. As displayed in Fig. 4(a), the V-$MoS_{2.49}$/CC delivers two distinct cathodic peaks centered at about 2.1 and 1.1 V during the first cathodic scan. The former is attributed to the reaction of bridge sulfur with Na^+ to form Na_2S, which is similar to the reaction in the Na-S battery system [36,37]. The latter peak is generally accepted as the intercalation of Na^+ into the MoS_2 interlayer to form the intercalation compound Na_xMoS_2 [14,38]. In particular, there is no peak associated with the further transformation of Na_xMoS_2, which avails the structure stability by preventing the irreversible conversion reaction. The above results indicate that the bridge sulfur can react with more Na^+ to contribute more capacity without destroying the intercalation-type reaction of MoS_2. Correspondingly, the two anodic peaks located at 1.5 and 2.4 V were detected during the first charge process, which belong to the deintercalation of Na^+ and the oxidation from Na_2S to bridge sulfur, respectively. It's worth noting that the curves overlap well after the first cycle, suggesting good reversibility. The *ex situ* XRD and Raman characterizations of the V-$MoS_{2.49}$/CC is also supplemented to demonstrate the reaction mechanism in a narrowed potential range of 0.4-3 V (Fig. S4 in the ESM). As shown in Fig. 4(b), the CV profiles scanned at rates ranging from 0.2 to 1.0 mV s^{-1} demonstrate that there are no significant variations in the peak shape and position, verifying fast reaction kinetics and high reversibility. In addition, the CV tests of the $MoS_{2.46}$/CC and MoS_2/CC without vanadium doping are also provided in Figs. 4(c)-4(d), respectively. One weak peak at 2.1 V can also be found in the initial discharge process of the $MoS_{2.46}$, in accordance with the V-$MoS_{2.49}$/CC. However, the $MoS_{2.46}$/CC delivers inferior invertibility, demonstrating that vanadium doping can enhance electrochemical activity of MoS_2 without changing its intrinsic reaction mechanism. As for MoS_2/CC, there is no visible cathodic peak at 2.1 V in the first cycle, which indicates that only the intercalation reaction occurs.

Fig. 5(a) provides the initial charge/discharge curves of the MoS_2/CC, $MoS_{2.46}$/CC and V-$MoS_{2.49}$/CC at 0.1 A g^{-1}. The V-$MoS_{2.49}$/CC shows a superior reversible capacity of 439 mAh g^{-1} with the highest initial Coulombic efficiency of 82%, which surpasses the pure MoS_2 (204 mAh g^{-1}, 62%) and $MoS_{2.46}$/CC (420 mAh g^{-1}, 71%). Moreover, the V-$MoS_{2.49}$ also shows decent rate capabilities, particularly at high rates (Fig. 5(b)). It can be observed that the capacity of V-$MoS_{2.49}$/CC exceeds that of the other samples at the whole range of current density, demonstrating a promising prospect as a high-performance anode for SIBs. Specifically, even at 10 A g^{-1}, it can still obtain a specific capacity up to 214 mAh g^{-1}. When resetting the current density to 0.1 A g^{-1}, the capacity of V-$MoS_{2.49}$/CC can be immediately restored. Fig. 5(c) shows the electrochemical impedance spectra (EIS) after rate-performance tests. The Nyquist plots of the V-$MoS_{2.49}$/CC present a much smaller semicircle in the high-frequency region and an oblique line in the low-frequency region, showing the lowest resistance, enhanced charge transfer kinetics and sodium-ion diffusion, which can be ascribed to the high conductivity derived from vanadium doping. In addition, the impedance comparison of the V-MoS_{2+x}/CC samples also prove the improved conductivity of the V-$MoS_{2.49}$/CC (see Fig. S5 in the ESM). The kinetics and quantitative analysis are further employed based on typical CV curves of the V-$MoS_{2.49}$/CC in Fig. 4(b) to verify pseudocapacitance-dominated contribution. The relationship of peak current (i) and scan rate (v) obeys the following power law: $i = a \cdot v^b$, where a and b represent the adjustable parameters [39,40]. Diffusion-controlled processes and surface-controlled capacitive behavior can be distinguished according to the calculated b values, in which b values equivalent to 0.5 and 1.0 represent diffusion-controlled process and surface-controlled capacitive behavior respectively. As shown in Fig. S6a in the ESM, the b values of three redox peaks are 1.0, 0.93 and 0.95, respectively, manifesting that capacitive behavior dominates the electrochemical process. The contributions of the capacity can be further quantified by the equation of $i = k_1v + k_2v^{1/2}$, where k_1v and $k_2v^{1/2}$ correspond to the current ratio from the capacitance- and diffusion-controlled reactions, respectively. Upon increasing the scan rate, the ratio of capacitive contribution becomes higher, and the capacitive contribution can reach 87% at 1.0 mV s^{-1} (Fig. 5(d) and Fig. S6b in

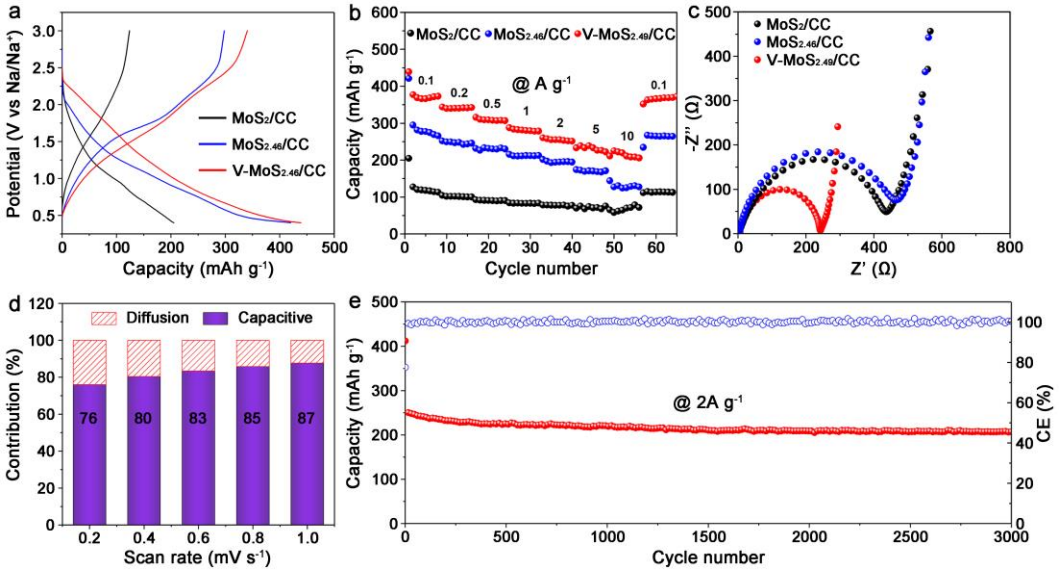

Figure ~~5~~ 6 (a) The initial charge/discharge profiles at 0.2 A g^{-1}, (b) rate capabilities at 0.1-10 A g^{-1}, and (c) Nyquist plots of the MoS_2/CC, the $MoS_{2.46}$/CC and the V-$MoS_{2.49}$/CC; (d) normalized capacity contribution ratio at 0.2-1.0 mV s^{-1} and (e) cycle life at 2.0 A g^{-1} of the V-$MoS_{2.49}$/CC.

the ESM). Therefore, the ultrahigh capacity and intriguing rate performance of the V-$MoS_{2.49}$/CC on the carbon cloth can be mainly attributed to its ultralow resistance and ultrahigh pseudocapacitance feature and vanadium doping. Intriguingly, the V-$MoS_{2.49}$/CC also achieves excellent cycling performance (Fig. 5(e)). The reversible capacity is kept at around 207 mAh g^{-1} (83% retention) with almost 100 % Coulombic efficiency after 3000 cycles at 2 A g^{-1}, which profits from the strong bridge sulfur S-S bonds and intercalation-reaction mechanism. To the best of our knowledge, the excellent rate capability of V-$MoS_{2.49}$/CC outperforms most of the state-of-the-art electrodes based on intercalation-type mechanism for SIBs (See Table S1 in the ESM). In addition, the SEM images (see Fig. S7 in the ESM) after the cycling test verify that the nanosheets are well retained, which is also a reflection of excellent reversibility.

4 Conclusions

In summary, we demonstrate the synthesis of the supersaturated bridge-sulfur and vanadium co-doped MoS_2 nanosheet arrays on the carbon cloth (V-MoS_{2+x}/CC) for constructing high-performance SIBs. The bridge-sulfur content can be controlled well by tuning the concentration of thioacetamide used in the synthesis, which works to facilitate new electrochemical active edges to offer extra sodium storage capacity. The natural conductivity of MoS_2 can be significantly enhanced resulting from the increase of electron density after vanadium doping. In addition, a pseudocapacitance-dominated reaction is clearly proved according to the kinetic and quantitative analysis, accounting for fast reaction kinetics. When used as an anode for SIBs, the optimized V-$MoS_{2.49}$/CC delivers a much higher capacity of 370 mAh g^{-1} at 0.1 A g^{-1} and 214 mAh g^{-1} at 10 A g^{-1} compared with the intercalation-type MoS_2 electrodes in the voltage range 0.4-3.0 V. More impressively, a durable cycling life of 3000 cycles can be achieved with a capacity retention of 83% at 2 A g^{-1}. Such edge-engineering and lattice-doping co-modification concept is a promising strategy to push the development of other metal sulfides-based electrode materials for high-performance SIBs.

Acknowledgements

The authors gratefully acknowledge the financial support from National Natural Science Foundation of China (51672082, 21975074 and 91534202), the Basic Research Program of Shanghai (17JC1402300), the Shanghai Scientific and Technological Innovation Project (18JC1410500), and the Fundamental Research Funds for the Central Universities (222201718002).

Electronic Supplementary Material: Supplementary material (further details of the SEM images, ex situ XRD and ex situ Raman spectroscopy measurements and electrochemical tests) is available in the online version of this article at http://dx.doi.org/10.1007/s12274-***-****-*.

References

[1] Li, K.; Zhang, J.; Lin, D.; Wang, D. W.; Li, B.; Lv, W.; Sun, S.; He, Y. B.; Kang, F.; Yang, Q. H. et al. Evolution of the electrochemical interface in sodium ion batteries with ether electrolytes. *Nat. Commun.* **2019**, *10*, 725.

[2] Wang, Y. X.; Chou, S. L.; Wexler, D.; Liu, H. K.; Dou, S. X. High-performance sodium-ion batteries and sodium-ion pseudocapacitors based on MoS_2/Graphene Composites. *Chem. Eur. J.* **2014**, *20*, 9607-9612.

[3] Song, X.; Wang, H.; Jin, S.; Lv, M.; Zhang, Y.; Kong, X.; Xu, H.; Ma, T.; Luo, X.; Tan, H. et al. Oligolayered $Ti_3C_2T_x$ MXene towards high performance lithium/sodium storage. *Nano Res.* **2020**, *13*, 1659-1667.

[4] Lu, J.; Zhao, S.; Fan, S.; Lv, Q.; Li, J.; Lv, R. Hierarchical SnS/SnS_2 heterostructures grown on carbon cloth as binder-free anode for superior sodium-ion storage. *Carbon* **2019**, *148*, 525-531.

[5] Edison, E.; Gogoi, P. K.; Zheng, Y.; Sreejith, S.; Pennycook, S. J.; Lim, C. T.; Srinivasan, M. Electrochemically induced amorphization and unique lithium and sodium storage pathways in $FeSbO_4$ nanocrystals. *ACS Appl. Mater. Interfaces* **2019**, *11*, 20082-20090.

[6] Ge, P.; Fouletier, M. Electrochemical intercalation of sodium in graphite. *Solid State Ionics* **1988**, *28*, 1172-1175.

[7] Slater, M. D.; Kim, D.; Lee, E.; Johnson, C. S. Sodium-ion batteries. *Adv. Funct. Mater.* **2013**, *23*, 947-958.

[8] Sun, D.; Ye, D.; Liu, P.; Tang, Y.; Guo, J.; Wang, L.; Wang, H. MoS_2/graphene nanosheets from commercial bulky MoS_2 and graphite as

anode materials for high rate sodium-ion batteries. *Adv. Energy Mater*. **2018**, *8*, 1702383.

[9] Deng, Z.; Jiang, H.; Li, C. 2D metal chalcogenides incorporated into carbon and their assembly for energy storage applications. *Small* **2018**, *14*, 1800148.

[10] Zhao X.; Wang G.; Liu X.; Zheng X.; Wang H. Ultrathin MoS_2 with expanded interlayers supported on hierarchical polypyrrole-derived amorphous N-doped carbon tubular structures for high-performance Li/Na-ion batteries. *Nano Res.* **2018**, *11*, 3603-3618.

[11] Chen, L.; Liu, Y.; Deng, Z.; Jiang, H.; Li, C. Edge-enriched MoS_2@C/rGO film as self-standing anodes for high-capacity and long-life lithium-ion batteries. *Sci. China Mater.* **2020**, https://doi.org/10.1007/s40843-020-1348-y.

[12] Yang, H.; Wang, M.; Liu, X.; Jiang, Y.; Yu, Y. MoS_2 embedded in 3D interconnected carbon nanofiber film as a free-standing anode for sodium-ion batteries. *Nano Res.* **2018**, *11*, 3844-3853.

[13] Hu, Z.; Wang, L.; Zhang, K.; Wang, J.; Cheng, F.; Tao, Z.; Chen, J. MoS_2 nanoflowers with expanded interlayers as high-performance anodes for sodium-ion batteries. *Angew. Chem. Int. Ed.* **2014**, *53*, 12794-12798.

[14] Park, J.; Kim, J.-S.; Park, J.-W.; Nam, T.-H.; Kim, K.-W.; Ahn, J.-H.; Wang, G.; Ahn, H.-J. Discharge mechanism of MoS_2 for sodium ion battery: Electrochemical measurements and characterization. *Electrochim. Acta* **2013**, *92*, 427-432.

[15] Xu, X.; Zhao, R.; Ai, W.; Chen, B.; Du, H.; Wu, L.; Zhang, H.; Huang, W.; Yu, T. Controllable design of MoS_2 nanosheets anchored on nitrogen-doped graphene: Toward fast sodium storage by tunable pseudocapacitance. *Adv. Mater*. **2018**, *30*, 1800658.

[16] Ding, Y. L.; Kopold, P.; Hahn, K.; Van Aken, P. A.; Maier, J.; Yu, Y. A lamellar hybrid assembled from metal disulfide nanowall arrays anchored on a carbon layer: In situ hybridization and improved sodium storage. *Adv. Mater.* **2016**, *28*, 7774-7782.

[17] Wang, H.; Jiang, H.; Hu, Y.; Saha, P.; Cheng, Q.; Li, C. Interface-engineered MoS_2/C nanosheet heterostructure arrays for ultra-stable sodium-ion batteries. *Chem. Eng. Sci.* **2017**, *174*, 104-111.

[18] Wang, Y.-X.; Seng, K. H.; Chou, S.-L.; Wang, J.-Z., Guo, Z.; Wexler, D., Liu, H.-K.; Dou, S.-X. Reversible sodium storage via conversion reaction of a MoS_2-C composite. *Chem. Commun.*, **2014**, *50*, 10730-10733.

[19] Lei, Z.; Zhan, J.; Tang, L.; Zhang, Y.; Wang, Y. Recent development of metallic (1T) phase of molybdenum disulfide for energy conversion and storage. *Adv. Energy Mater*. **2018**, *8*, 1703482.

[20] Liu, Y.; Wang, X.; Song, X.; Dong, Y.; Yang, L.; Wang, L.; Jia, D.; Zhao, Z.; Qiu, J. Interlayer expanded MoS_2 enabled by edge effect of graphene nanoribbons for high performance lithium and sodium ion batteries. *Carbon* **2016**, *109*, 461-471.

[21] Li, Y.; Yu, Y.; Huang, Y.; Nielsen, R. A.; Goddard III, W. A.; Li, Y.; Cao, L. Engineering the composition and crystallinity of molybdenum sulfide for high-performance electrocatalytic hydrogen evolution. *ACS Catal.* **2015**, *5*, 448-455.

[22] Lee, C.-H.; Lee, S.; Kang, G.-S.; Lee, Y.-K.; Park, G. G.; Lee, D. C.; Joh, H.-I. Insight into the superior activity of bridging sulfur-rich amorphous molybdenum sulfide for electrochemical hydrogen evolution reaction. *Appl. Catal., B* **2019**, *258*, 117995.

[23] Wang, C.; Wang, H.; Hu, X.; Matios, E.; Luo, J.; Zhang, Y.; Lu, X.; Li, W. Frogspawn-coral-like hollow sodium sulfide nanostructured cathode for high-rate performance sodium-sulfur batteries. *Adv. Energy Mater.* **2019**, *9*, 1803251.

[24] Bao, W.; Shuck, C. E.; Zhang, W.; Guo, X.; Gogotsi, Y.; Wang, G. Boosting performance of Na-S batteries using sulfur-doped $Ti_3C_2T_x$ MXene nanosheets with a strong affinity to sodium polysulfides. *ACS Nano* **2019**, *13*, 11500-11509.

[25] Yang, T.; Guo, B.; Du, W.; Aslam, M. K.; Tao, M.; Zhong, W.; Chen, Y.; Bao, S.-J.; Zhang, X.; Xu, M. Design and construction of sodium polysulfides defense system for room-temperature Na-S battery. *Adv. Sci.* **2019**, *6*, 1901557.

[26] Fang, Y.; Yu, X. Y.; Lou, X. W. Formation of hierarchical Cu-doped $CoSe_2$ microboxes via sequential ion exchange for high-performance sodium-ion batteries. *Adv. Mater.* **2018**, *30*, 1706668.

[27] Xiong, Q.; Wang, Y.; Liu, P. oF.; Zheng, L. R.; Wang, G.; Yang, H. G.; Wong, P. K.; Zhang, H.; Zhao, H. Cobalt covalent doping in MoS_2 to induce bifunctionality of overall water splitting. *Adv. Mater.* **2018**, *30*, 1801450.

[28] Liu, H.; He, Q.; Jiang, H.; Lin, Y.; Zhang, Y.; Habib, M.; Chen, S.; Song, L. Electronic structure reconfiguration toward pyrite NiS_2 via engineered heteroatom defect boosting overall water splitting. *ACS nano* **2017**, *11*, 11574-11583.

[29] Higgins, D.; Hoque, M. A.; Seo, M. H.; Wang, R.; Hassan, F.; Choi, J. Y.; Pritzker, M.; Yu, A.; Zhang, J.; Chen, Z. Development and simulation of sulfur-doped graphene supported platinum with exemplary stability and activity towards oxygen reduction. *Adv. Funct. Mater*. **2014**, *24*, 4325-4336.

[30] Wang, X. L.; Li, G.; Seo, M. H.; Hassan, F. M.; Hoque, M. A.; Chen, Z. W. Sulfur atoms bridging few-layered MoS_2 with S-doped graphene enable highly robust anode for lithium-ion batteries. *Adv. Energy Mater.* **2015**, *5*, 1501106.

[31] Acerce, M.; Voiry, D.; Chhowalla, M. Metallic 1T phase MoS_2 nanosheets as supercapacitor electrode materials. *Nat. Nanotechnol.* **2015**, *10*, 313.

[32] Xu, Q.; Liu, Y.; Jiang, H., Hu, Y.; Liu, H.; Li, C. Unsaturated sulfur edge engineering of strongly coupled MoS_2 nanosheet-carbon macroporous hybrid catalyst for enhanced hydrogen generation. *Adv. Energy Mater.* **2019**, *9*, 1802553.

[33] He, P.; Yan, M.; Zhang, G.; Sun, R.; Chen, L.; An, Q.; Mai, L. Layered VS_2 nanosheet-based aqueous Zn ion battery cathode. *Adv. Energy Mater.* **2017**, *7*, 1601920.

[34] Xia, S.; Wang, Y.; Liu, Y.; Wu, C.; Wu, M.; Zhang, H. Ultrathin MoS_2 nanosheets tightly anchoring onto nitrogen-doped graphene for enhanced lithium storage properties. *Chem. Eng. J.* **2018**, *332*, 431-439.

[35] Li, B.; Qiao, S.; Zheng, X.; Yang, X.; Cui, Z.; Zhu, S.; Li, Z.; Liang, Y. Pd coated MoS_2 nanoflowers for highly efficient hydrogen evolution reaction under irradiation. *J. Power Sources* **2015**, *284*, 68-76.

[36] Du, W.; Wu, Y.; Yang, T.; Guo, B.; Liu, D.; Bao, S.-J.; Xu, M. Rational construction of rGO/VO_2 nanoflowers as sulfur multifunctional hosts for room temperature Na-S batteries. *Chem. Eng. J.* **2020**, *379*, 122359.

[37] Wang, Y.-X.; Yang, J.; Lai, W.; Chou, S.-L.; Gu, Q.-F.; Liu, H. K.; Zhao, D.; Dou, S. X. Achieving high-performance room-temperature sodium-sulfur batteries with S@interconnected mesoporous carbon hollow nanospheres. *J. Am. Chem. Soc.* **2016**, *138*, 16576-16579.

[38] Choi, S. H.; Ko, Y. N.; Lee, J. K.; Kang, Y. C. 3D MoS_2-graphene microspheres consisting of multiple nanospheres with superior sodium ion storage properties. *Adv. Funct. Mater.* **2015**, *25*, 1780-1788.

[39] Chen, L.; Jiang, H.; Hu, Y.; Wang, H.; Li, C. In-situ growth of ultrathin MoS_2 nanosheets on sponge-like carbon nanospheres for lithium-ion batteries. *Sci. China Mater.* **2018**, *61*, 1049-1056.

[40] Ma, Y.; Ma, Y.; Bresser, D.; Ji, Y.; Geiger, D.; Kaiser, U.; Streb, C.; Varzi, A.; Passerini, S. Cobalt disulfide nanoparticles embedded in porous carbonaceous micro-polyhedrons interlinked by carbon nanotubes for superior lithium and sodium storage. *ACS Nano* **2018**, *12*, 7220-7231.